Gravity compensation for impedance control of legged robots using optimizationless proportional contact force estimation

Christopher Yee Wong, *Member, IEEE,*, Ko Ayusawa, *Member, IEEE,* and Eiichi Yoshida, *Member, IEEE*

***Abstract*— Impedance control of humanoid robots, a form of compliant control, allows them to move in a fashion similar to humans and increase the safety of interactions with humans or the environment. In low stiffness impedance control, gravitational forces will cause the robot to deviate significantly from the desired position. Thus, a gravity compensation term in the joint motor torque command is required to counteract gravitational forces. Ground reaction forces are sometimes used to estimate the gravity compensation torque required for each joint. In this paper, a novel method to estimate contact forces by using model mass properties and relative force and torque sensor data of each contact point with respect to all loaded limbs is proposed. This simple and straightforward method, called the proportional method, is able to resolve internal forces arising from closed-loop kinematic chains in multi-contact situations, for example the double support phase of bipedal robots, without optimization. The proposed method is also more robust to sensor error and is able to implicitly distinguish between gravitational and external forces for impedance control. Simulations and experiments using the humanoid robot HRP-4 are performed to validate the proposed method.**

I. Introduction

Humanoid robots, shown in Fig. 1, have wide applications, for example in social care [1], manufacturing [2], and entertainment [3]. Humanoid robot control aims to move the robot in more human-like fashion using the whole body, rather than just isolated body parts. This is highlighted by advances in retargeting whole-body human motion for humanoid robots, performing dances [3], or mimicking a lifting motion to use humanoid robots as an evaluation platform of wearable assistive devices [4]–[6]. These motions, although human-like, are performed using stiff high-gain position control. While position control performs well for isolated motions, it can be dangerous if there are any unintended collisions. Compliant control of rigid-joint robots, on the other hand, provides a softer interaction paradigm closer to that of human motion by dictating an interaction force around a desired position, and can naturally absorb impact with less harmful consequences [7]. Thus, for humanoid robot motion to become more human-like or to achieve safer physical human-robot interaction, compliant control is more appropriate [8].

Impedance control, a form of compliant control, combines position and force control in a way that specifies a force output as a result of input motion [9]. The applied motor torque from an impedance controller $\boldsymbol{\tau}_{imp}$ is governed by Eq. (1). The system response is shaped to exhibit motion according to desired stiffness $\boldsymbol{K}_d$ and damping $\boldsymbol{D}_d$ coefficients when the actual joint positions $\boldsymbol{q}$ and velocities $\dot{\boldsymbol{q}}$ deviate from the reference joint positions $\boldsymbol{q}_d$ and velocities $\dot{\boldsymbol{q}}_d$. Inertial shaping is also possible, but is omitted to simplify calculations.

C. Y. Wong is a postdoctoral fellow, and K. Ayusawa and E. Yoshida are researchers with the Intelligent Systems Research Institute at the National Institute of Advanced Industrial Science and Technology (AIST), Tsukuba, Ibaraki, Japan. Contact emails: cy.wong@aist.go.jp, k.ayusawa@aist.go.jp and e.yoshida@aist.go.jp

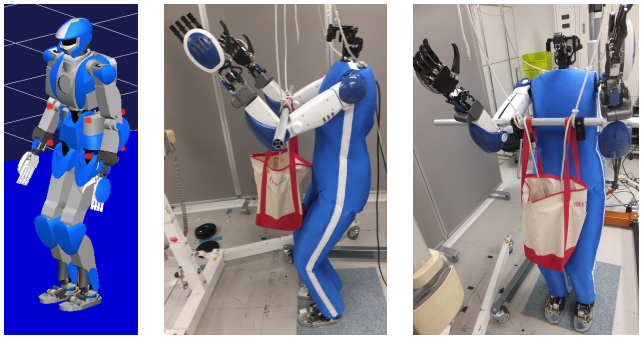

(a) (b) (c)

Fig. 1. Humanoid robot HRP-4 in a) Choreonoid simulation, and b) experimental setup side view and c) front view

$$\boldsymbol{D}_d(\dot{\boldsymbol{q}} - \dot{\boldsymbol{q}}_d) + \boldsymbol{K}_d(\boldsymbol{q} - \boldsymbol{q}_d) = \boldsymbol{\tau}_{imp} \tag{1}$$

Generalized system dynamics are defined by Eq. (2) with floating base link combined position and orientation $\boldsymbol{x}$, system inertia $\boldsymbol{I}$, bias forces $\boldsymbol{C}$ including Coriolis and centrifugal forces, gravitational forces $\boldsymbol{F}_g$ and torques $\boldsymbol{\tau}_g$, motor torque $\boldsymbol{\tau}_m$, contact forces $\boldsymbol{F}_j$ where $j \in 1...m$, and the Jacobian $\boldsymbol{J}$ with respect to contact j [10]. Subscripts b and q identify if a variable is with respect to the robot base link or joints:

$$\boldsymbol{I}\begin{bmatrix}\ddot{\boldsymbol{x}}\\ \ddot{\boldsymbol{q}}\end{bmatrix} + \begin{bmatrix}\boldsymbol{C}_b + \boldsymbol{F}_g\\ \boldsymbol{C}_q + \boldsymbol{\tau}_g\end{bmatrix} = \begin{bmatrix}0\\ \boldsymbol{\tau}_m\end{bmatrix} + \sum_{j=1}^{m}\begin{bmatrix}\boldsymbol{J}_{b,j}^T\\ \boldsymbol{J}_{q,j}^T\end{bmatrix}\boldsymbol{F}_j \tag{2}$$

For many robotic tasks, tracking a desired reference position or trajectory in space is an important criterion. In gravity-affected systems using only impedance control (i.e.: $\boldsymbol{\tau}_m = \boldsymbol{\tau}_{imp}$), high stiffness gains $\boldsymbol{K}_d$ are required for accurate unloaded position tracking. However, this is counter-productive to compliant control. The addition of a feedforward gravity compensation term $\boldsymbol{\tau}_{gc}$ to motor input $\boldsymbol{\tau}_m$, in Eq. (3), is used to counteract gravitational forces τ_g [11]. Inclusion of $\boldsymbol{\tau}_{gc}$ allows using lower $\boldsymbol{K}_d$ in the impedance controller to achieve softer compliance while maintaining accurate unloaded position tracking.

$$\boldsymbol{\tau}_m = \boldsymbol{\tau}_{imp} + \boldsymbol{\tau}_{gc} \tag{3}$$

Ground reaction forces (GRF), the forces exerted on the robot from the ground or contact surface, can be used to determine $\boldsymbol{\tau}_{gc}$, but can be difficult with multiple contact points that form closed-loop kinematic chain, as internal forces must be resolved. GRF can be measured directly using force and torque (F/T) sensors [11], [12], or estimated using optimization [13], [14] or proprioceptive data with model properties [15]. Contact force estimation is a well studied topic, and while optimization and model-based methods are widely used, they can be difficult and daunting for users who do not have any prior experience.

The focus of this paper is a novel method for the derivation of the gravity compensation term $\boldsymbol{\tau}_{gc}$ for impedance control of bipedal humanoid robots through estimation of the GRF using F/T sensors. The proposed method does not directly use the F/T sensor values, but rather combines model mass properties with the proportional loading of each contact point versus the total contact forces across all limbs. This proportional method is simple and straightforward to implement, while able to resolve the internal forces of multiple contact points without resorting to optimization, and is more robust to F/T sensor noise and calibration errors. Most importantly, it is able to implicitly distinguish between gravitational forces $\boldsymbol{\tau}_g$ and external forces $\boldsymbol{\tau}_{ext}$, which is paramount for impedance control. This paper represents the preliminary steps towards the goal of impedance-based whole body control of a humanoid robot.

The breakdown of this paper is as follows: gravity compensation and the proposed proportional method are described in detail in Section II. In Section III, the proposed method and another F/T sensor-based GRF estimation method are tested both in simulation and on the humanoid robot HRP-4 for impedance control, and the results are discussed. Concluding remarks are made in Section IV.

II. Gravity Compensation Estimation

A. Gravity compensation estimation calculation

Gravity compensation, as the name implies, is a matter of balancing gravitational forces with the applied motor torque. In multi-contact floating base systems, for example bipedal robots, weight distribution amongst the contact points must be taken into account when calculating GRFs. These GRFs can then be used to open the kinematic chain for calculating $\boldsymbol{\tau}_{gc}$ for each joint in that limb according to Fig. 2. A contact force is assumed to be at the most distal point of the limb, but may be measured somewhere else instead, as shown in Fig. 2(a). For both single and multi-contact cases, gravity compensation torque $\tau_{gc,i}$ for joint i is calculated using Eq. (4), detailed in Fig. 2(b). The following notation is used: subscript $i \in 1...n$ refers to individual joints, and subscript $j \in 1...m$ refers to individual contact points. It is assumed that there is only one contact point per limb. Joint torques use the Greek letter τ_i, whereas torques located at contact points are marked with capital $\boldsymbol{T}_j$.

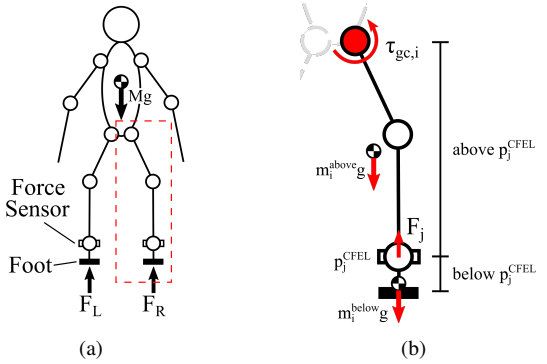

Fig. 2. a) Overall contact force distribution and sensor layout, and b) gravity compensation estimation $\tau_{gc,i}$ calculation

$$\begin{aligned} \tau_{gc,i} &= (\boldsymbol{p}_i^j \times \boldsymbol{F}_j + \boldsymbol{T}_j + \boldsymbol{p}_i^{\text{COM,above}} \times m_i^{\text{above}} \boldsymbol{g}) \cdot \boldsymbol{a}_i \\ m_i^{\text{above}} &= m_i^{\text{sub}} - m_i^{\text{below}} \\ \boldsymbol{p}_i^{\text{COM,above}} &= \frac{\boldsymbol{p}_i^{\text{COM,sub}} m_i^{\text{sub}} - \boldsymbol{p}_i^{\text{COM,below}} m_i^{\text{below}}}{m_i^{\text{above}}} \end{aligned} \tag{4}$$

Where $\boldsymbol{p}_i^j$ is the position from joint i to the j^{th} contact force estimation location (CFEL) $\boldsymbol{p}_j^{\text{CFEL}}$ (e.g.: location of F/T sensor); $\boldsymbol{F}_j$ and $\boldsymbol{T}_j$ are respectively the contact force and torque at $\boldsymbol{p}_j^{\text{CFEL}}$; m_i^{sub} is the mass distal of joint i; m_i^{above} is the mass distal of joint i but proximal of $\boldsymbol{p}_j^{\text{CFEL}}$; m_i^{below} is the mass distal of $\boldsymbol{p}_j^{\text{CFEL}}$; $\boldsymbol{p}_i^{\text{COM,sub}}$ is the position from joint i to center of mass (COM) of m_i^{sub}; similarly $\boldsymbol{p}_i^{\text{COM,above}}$ and $\boldsymbol{p}_i^{\text{COM,below}}$ are the positions from joint i to COM of m_i^{above} and m_i^{below} respectively; $\boldsymbol{g}$ is the gravity vector; and $\boldsymbol{a}_i$ is the joint axis vector of joint i. Unless specified, all values are expressed in the robot base link frame. Initial experiments attempted to only used model properties to calculate gravity compensation, while ignoring internal or loop forces. This open loop approach resulted in errors in gravity compensation estimation, demonstrating that internal forces cannot be ignored in multi-contact situations, requiring the methods described below.

B. Ground reaction force estimation using direct sensor method

Multi-contact systems form closed-loop kinematic chains, and thus internal forces that are difficult to resolve algebraically may be present in the GRF. As mentioned in Section I, there are many methods to resolving the internal forces of the GRF when multiple contact points are present. In this paper, we will focus on methods that use F/T sensors. F/T sensors allow the contact forces, along with the internal forces, to be measured directly as $\boldsymbol{F}_j^s$ and $\boldsymbol{T}_j^s$. The superscript s denotes that this estimation is obtained by directly using the sensor values. Joint gravity compensation torque using the *direct sensor method* $\tau_{gc,i}^s$ is calculated by substituting the GRF values $\boldsymbol{F}_j$ and $\boldsymbol{T}_j$ in Eq. (4) with the direct F/T sensor measurements $\boldsymbol{F}_j^s$ and $\boldsymbol{T}_j^s$ as shown in Eq. (5). The direct sensor method is the most straightforward method when F/T sensors are used to estimate the GRF.

$$\tau^s_{gc,i} = (\boldsymbol{p}^j_i \times \boldsymbol{F}^s_j + \boldsymbol{T}^s_j + \boldsymbol{p}^{\text{COM,above}}_i \times m^{\text{above}}_i \boldsymbol{g}) \cdot \boldsymbol{a}_i \quad (5)$$

C. Ground reaction force estimation using proportional method

Proper calibration of F/T sensors is a difficult and time-consuming process. If performed improperly, absolute F/T sensor data may not be trustworthy or accurate. To alleviate this issue, a novel method is proposed that employs F/T sensors, but does not use the sensor data directly. Instead, the proportional GRF of each limb relative to the total GRF across all limbs is used. This proportion is then combined with model data to calculate GRFs. Hence, we call this the *proportional method*, denoted by the superscript p. Contact force $\boldsymbol{F}^p_j$ is estimated first, then used to estimate contact torque $\boldsymbol{T}^p_j$. The methods proposed here are valid for both single- and multi-support phases.

Prior to estimation, the first step is to modify the frame in which the following analyses will be performed. Certain variables, for example those in Eq. (6), are multiplied by rotation matrices $\boldsymbol{R}^f$ and $\boldsymbol{R}^t$ when estimating contact forces and torques. Depending on which rotation matrix is used, rotated variables are denoted with tilde and hat accents. The purpose of change in reference frame and the definition of rotation matrices are explained in Section II-D.

$$\begin{aligned} \tilde{\boldsymbol{F}}^s_j &= \boldsymbol{R}^f \boldsymbol{F}^s_j,\ \tilde{\boldsymbol{g}} = \boldsymbol{R}^f \boldsymbol{g} \\ \hat{\boldsymbol{F}}^s_j &= \boldsymbol{R}^t \boldsymbol{F}^s_j,\ \hat{\boldsymbol{T}}^s_j = \boldsymbol{R}^t \boldsymbol{T}^s_j \end{aligned} \quad (6)$$

Contact force and torque proportionality coefficients, $\alpha^s_{j,k}$ and $\beta^s_{j,k}$ respectively, are calculated for each contact point j in each axis $k \in x, y, z$, according to Eq. (7):

$$\alpha^s_{j,k} = \frac{\tilde{F}^s_{j,k}}{\sum_{j=1}^{m} |\tilde{F}^s_{j,k}|},\ \beta^s_{j,k} = \frac{\tilde{T}^s_{j,k}}{\sum_{j=1}^{m} |\tilde{T}^s_{j,k}|} \text{ for } k \in x, y, z \quad (7)$$

Where $|\cdot|$ is the absolute value. Note that these coefficients retain the directionality of the contact force, such that $-1 \leq \alpha^s_{j,k}, \beta^s_{j,k} \leq 1$. For ease of notation, proportionality matrices $\boldsymbol{\alpha}^s_j$ and $\boldsymbol{\beta}^s_j$ can be formed by placing the elements in a diagonal matrix $\boldsymbol{\alpha}^s_j = \text{diag}(\begin{bmatrix}\alpha^s_{j,x} & \alpha^s_{j,y} & \alpha^s_{j,z}\end{bmatrix})$ and $\boldsymbol{\beta}^s_j = \text{diag}(\begin{bmatrix}\beta^s_{j,x} & \beta^s_{j,y} & \beta^s_{j,z}\end{bmatrix})$.

Contact forces are estimated with the assumption of static conditions, such that dynamic effects are ignored. Thus, the upper portion of Eq. (2) becomes $\boldsymbol{F}_g = \sum_{j=1}^{m} \boldsymbol{J}^T_{b,j} \boldsymbol{F}_j$. By using lumped mass parameters at the center of mass $\boldsymbol{F}_g = m\tilde{\boldsymbol{g}}$, and putting it in context of the proportional method where $\boldsymbol{J}^T_{b,j} \boldsymbol{F}_j = \tilde{\boldsymbol{F}}^p_j$, this equation becomes $m\tilde{\boldsymbol{g}} = \sum_{j=1}^{m} \tilde{\boldsymbol{F}}^p_j$. For multi-contact scenarios, this equation has infinite number of solutions, as we are trying to estimate the contact forces $\tilde{\boldsymbol{F}}^p_j$. Instead, we observe the resulting summation $\tilde{\boldsymbol{F}}^{\text{diff}} = \Sigma_{j=1}^{m} \tilde{\boldsymbol{F}}^p_j$, leading to Eq. (8):

$$m\tilde{\boldsymbol{g}} = \tilde{\boldsymbol{F}}^{\text{diff}} \quad (8)$$

Since $\tilde{\boldsymbol{F}}^{\text{diff}}$ sums the contact forces, the presence of opposite forces will lower the magnitude of the resultant summation. Dividing by the proportionality coefficients aids in recovering missing opposing internal forces, as in Eq. (9):

$$\tilde{F}^{\text{tot}}_k = \frac{\tilde{F}^{\text{diff}}_k}{|\sum_{j=1}^{m} \alpha^s_{j,k}|} \text{ for } k \in x, y, z \quad (9)$$

Recall that the coefficients $\alpha^s_{j,k}$ contain directionality. The use of the absolute modifier outside of the summation in the denominator, combined with the fact that the coefficients can be positive or negative, means that forces in opposite directions will result in summations less than one. Thus, $\tilde{F}^{\text{tot}}_k \geq F^{\text{diff}}_k$. This step allows resolution of the internal forces lost in the transition to Eq. (8). $\tilde{F}^{\text{tot}}_k$ represents the summation of the magnitude of all contact forces in axis k. Individual contact forces are then reconstructed by multiplying the total force $\tilde{\boldsymbol{F}}^{\text{tot}}$ with the proportionality coefficient, and then multiplying by the transpose of the rotation matrix $\boldsymbol{R}^{\text{f}}$:

$$\boldsymbol{F}^p_j = (\boldsymbol{R}^{\text{f}})^T \tilde{\boldsymbol{F}}^p_j,\ \tilde{\boldsymbol{F}}^p_j = \boldsymbol{\alpha}^s_j \tilde{\boldsymbol{F}}^{\text{tot}} \quad (10)$$

Contact torques $\boldsymbol{T}^p_j$ estimated using the proportional method are performed in a similar fashion as above. The moment balance with respect to the center of mass for a static case is written in Eq. (11):

$$0 = \sum_{j=1}^{m} (\hat{\boldsymbol{T}}^p_j + \hat{\boldsymbol{r}}_j \times \hat{\boldsymbol{F}}^p_j) \quad (11)$$

Where $\hat{\boldsymbol{r}}_j = \boldsymbol{R}^t \boldsymbol{r}_j$ is the position vector from the center of mass to the j^{th} contact point in the rotated reference frame. Similar to contact force estimation, what is observed in reality is only resultant summation of moments:

$$\sum_{j=1}^{m} \hat{\boldsymbol{T}}^p_j = \hat{\boldsymbol{T}}^p_{\text{diff}} = -\sum_{j=1}^{m} (\hat{\boldsymbol{r}}_j \times \hat{\boldsymbol{F}}^p_j) \quad (12)$$

Similar to above, total torque $\hat{T}^{\text{tot}}_k$ is reconstructed by dividing by the summation of proportionality coefficients in Eq. (13), and individual contact torques $\boldsymbol{T}_j$ by multiplying by the respective proportionality coefficient first, then the rotation frame $\boldsymbol{R}^t$ transposed, as shown Eq. (14):

$$\hat{T}^{\text{tot}}_k = \frac{\hat{T}^{\text{diff}}_k}{|\sum_{j=1}^{m} \beta^s_{j,k}|} \text{ for } k \in x, y, z \quad (13)$$

$$\boldsymbol{T}_j = (\boldsymbol{R}^t)^T \hat{\boldsymbol{T}}_j,\ \hat{\boldsymbol{T}}_j = \boldsymbol{\beta}^{\text{s}}_j \hat{\boldsymbol{T}}^{\text{tot}} \quad (14)$$

Thus, the joint gravity compensation torque $\tau^p_{gc,i}$ is calculated using Eq. (15), derived from Eq. (4):

$$\tau^p_{gc,i} = (\boldsymbol{p}^j_i \times \boldsymbol{F}^p_j + \boldsymbol{T}^p_j + \boldsymbol{p}^{\text{COM,above}}_i \times m^{\text{above}}_i \boldsymbol{g}) \cdot \boldsymbol{a}_i \quad (15)$$

Although the contact model is not explicitly restricted to being unilateral, as is typical for legged locomotion, the proportionality F/T coefficients approach zero as contact is

lost, acting as a pseudo-unilateral contact model. To further remove ambiguity, sensor values opposing gravity below a threshold are not considered to be in contact and are ignored in GRF calculations (e.g.: a foot pushing up on an object is not considered in contact for GRF calculation purposes.

D. Rotation matrices $\boldsymbol{R}^f$ and $\boldsymbol{R}^t$

The purpose of the rotation matrices $\boldsymbol{R}^f$ and $\boldsymbol{R}^t$ is to mitigate situations in Eqs. (9) and (13) where the denominators $\sum_{j=1}^{m} \alpha_{j,k}^s \approx 0$ or $\sum_{j=1}^{m} \beta_{j,k}^s \approx 0$ for one or two, but not all, axes $k \in x, y, z$, thus generating unstable values of $\boldsymbol{F}^{\text{tot}}$ and $\boldsymbol{T}^{\text{tot}}$. This situation occurs when there are forces or moments that are equal in magnitude but opposite in direction in a specific axis, but the vector-level summation is non-zero. To alleviate this problem, rotation matrices $\boldsymbol{R}^f$ and $\boldsymbol{R}^t$ are generated to rotate the summations $\Delta\boldsymbol{F}^s$ and $\Delta\boldsymbol{T}^s$, according to Eq. (6), to point along unit vector $\hat{\boldsymbol{e}} = \frac{\boldsymbol{e}}{\|\boldsymbol{e}\|}$, where $\boldsymbol{e} = \begin{bmatrix}1 & 1 & 1\end{bmatrix}^T$ and $\|\cdot\|$ is the Euclidean norm. These rotations redistribute the overall summation magnitude across all axes so that no single axis is close to zero. Thus, denominator terms $\sum_{j=1}^{m} \alpha_{j,k}^s \not\approx 0$ or $\sum_{j=1}^{m} \beta_{j,k}^s \not\approx 0$ for all axes $k \in x, y, z$. The result is that Eqs. (9) and (13) stabilize as risk of near zero denominators is significantly lowered. Rotation axis $\boldsymbol{u}$ and angle θ are defined in Eq. (16), and used to calculate the rotation matrix defined in Eq. (17). Note that rotation axis $\boldsymbol{u}$ and angle θ are recalculated for $\boldsymbol{R}^f$ and $\boldsymbol{R}^t$ using their respective F/T sensor values.

$$\begin{aligned} \boldsymbol{u} &= \text{sgn}(\Phi)\Phi \times \hat{\boldsymbol{e}},\ \Phi \in \Delta F^s, \Delta T^s \\ \theta &= \sin^{-1}\left(\frac{\|\boldsymbol{u}\|}{\|\Phi\|\|\hat{\boldsymbol{e}}\|}\right) + \frac{1 - \text{sgn}(\Phi)}{2}\pi \end{aligned} \tag{16}$$

$$\boldsymbol{R} = \begin{bmatrix} \text{c}_\theta + u_x^2\gamma & u_{xy}\gamma + u_z\text{s}_\theta & u_{xz}\gamma - u_y\text{s}_\theta \\ u_{xy}\gamma - u_z\text{s}_\theta & \text{c}_\theta + u_y^2\gamma & u_{yz}\gamma + u_x\text{s}_\theta \\ u_{xz}\gamma + u_y\text{s}_\theta & u_{yz}\gamma - u_x\text{s}_\theta & \text{c}_\theta + u_z^2\gamma \end{bmatrix} \tag{17}$$

$$\begin{gathered} u_{xy} = u_x u_y\ ,\ u_{xz} = u_x u_z\ ,\ u_{yz} = u_y u_z \\ \gamma = 1 - \text{c}_\theta\ ,\ \text{c}_\theta = \cos\theta\ ,\ \text{s}_\theta = \sin\theta \end{gathered}$$

E. Special requirement for impedance control

Since the method presented in this paper uses the contact forces of closed kinematic chains to calculate $\boldsymbol{\tau}_{gc}$, it is important to be able to distinguish between gravitational $\boldsymbol{\tau}_g$ and external forces $\boldsymbol{\tau}_{ext}$ within the contact forces for the purpose of impedance control. In Eq. (3), $\boldsymbol{\tau}_m$ is split into its constituents $\boldsymbol{\tau}_{imp}$ and $\boldsymbol{\tau}_{gc}$. In an ideal situation, these constituents perfectly represent their counterparts $\boldsymbol{\tau}_{gc} = \boldsymbol{\tau}_g$ and $\boldsymbol{\tau}_{imp} := \boldsymbol{D}_d(\dot{\boldsymbol{q}} - \dot{\boldsymbol{q}}_d) + \boldsymbol{K}_d(\boldsymbol{q} - \boldsymbol{q}_d) = \boldsymbol{\tau}_{ext}$. This is an important distinction as $\boldsymbol{\tau}_{gc}$ allows improved steady-state unloaded position tracking, while $\boldsymbol{\tau}_{imp}$ dictates the dynamic response to external forces.

While the direct sensor method is able to resolve internal forces, it cannot distinguish between external forces and gravitational forces. Both are merged together in the sensor data and treated as $\boldsymbol{\tau}_{gc}^s = \boldsymbol{\tau}_g + \boldsymbol{\tau}_{ext}$, resulting in $\boldsymbol{\tau}_{imp} = 0$. Thus, making it unsuitable for gravity compensation estimation in impedance control. Further steps would be required to allow the direct sensor method to be able to distinguish between the two forces, for example by including a model-based contact force estimation, but are beyond the scope of this paper. Conversely, the proposed proportional method, by virtue of using model properties and not absolute F/T sensor values to calculate contact forces, is unaffected by external forces when determining $\boldsymbol{\tau}_{gc}$. Thus, the proportional method is able to implicitly distinguish between $\boldsymbol{\tau}_g$ and $\boldsymbol{\tau}_{ext}$, making it suitable for impedance control. This difference is illustrated in Section III.

III. Results

A. HRP-4 Robot

The humanoid robot HRP-4 [16], shown in Fig. 1, is used for experimental validation of the proposed method. HRP-4 has an anthropomorphic body with a total of 37 rigid-joint degrees of freedom (DOF): two arms (9 DOF each), two legs (7 DOF each), a torso (3 DOF) and a head (2 DOF). It is designed to mimic the average Japanese woman at a height of 1514 mm and weight of 39 kg. On-board sensors include an inertial measurement unit (IMU) located in the waist link, and six-axis F/T sensors located on each leg just below the ankle joint, but above the foot and toe links, as shown in Fig. 2(a). Thus, the F/T sensors are not directly in contact with the ground, and mass exists below the sensors. The HRP-4 robot used is a modified version of the standard commercial HRP-4 model, where the hard shell is replaced with a soft foam shell to further mimic the physical form of a human.

B. Simulation

Choreonoid simulation environment [Fig. 1(a)] is used to verify the accuracy and compare the direct sensor τ_{gc}^s and the proportional τ_{gc}^p gravity compensation torque estimation methods. Although both methods accurately estimate the torque required for gravity compensation when compared to joint torque readouts in different static postures, performance differences exist when the methods are subjected to different types of sensor error. Three cases are used:

1) Addition of zero mean, uniformly distributed noise to both left/right sensors (20 N peak-to-peak amplitude for force values, and 3 Nm amplitude for torque values)
2) Constant rotation offset of F/T sensor values for right foot only to simulate improper sensor calibration or mounting (5° offset in each roll, pitch and yaw axis)
3) Scaling offset of right foot F/T sensor values by 1.2x

In all test cases, the robot is kept static in a neutral position shown in Fig. 1(a), and the actual knee joint torque τ and the gravity compensation estimations using the direct sensor τ_{gc}^s and proportional methods τ_{gc}^p are compared. The different sensor error types are applied one at a time, and two parameters, mean torque and signal variance, are measured over 3 seconds (at 200 Hz) and tabulated in Table I. τ_{gc}^s and τ_{gc}^p calculations both use the same modified F/T sensor values. In the case of sensor error type 1 with zero-mean noise, both τ_{gc}^s and τ_{gc}^p have similar mean torque values compared to the actual torque readout τ, but 63% reduction in signal variance when using the proportional method compared to the direct sensor method. For both error types 2 and 3, rotation offset

TABLE I

EFFECT OF SENSOR ERROR ON RIGHT KNEE GRAVITY COMPENSATION TORQUE ESTIMATIONS

Sensor Error Type	Actual τ Mean	Actual τ Var $\times 10^{-5}$	Direct sensor τ^s_{gc} Mean	Direct sensor τ^s_{gc} Var $\times 10^{-5}$	Proportional τ^p_{gc} Mean	Proportional τ^p_{gc} Var $\times 10^{-5}$
Baseline	**-20.03**	**3.33**	**-20.11**	**11.0**	**-20.02**	**0.091**
Noise	-20.03	97.8	-19.33	498774	-20.16	186787
Rotation	-20.07	0.78	-25.58	14.90	-22.57	3.18
Scaling	-19.95	2.05	-24.55	15.13	-21.96	5.32

and scaling offset, errors in mean torque are also reduced when using the proportional method compared to the direct sensor method. A special property of the proportional method is that if any type of error affects all F/T sensors in the same manner, then the error is nullified as the proportional method examines the relative differences between the F/T sensor values.

As stated above, the direct sensor method of gravity compensation is unable to distinguish between gravitational and external forces, which is required for impedance control. Fig. 3(b) demonstrates this issue where a load is applied to impedance-controlled knee joints at $t = 4$ s. Using the proportional gravity compensation estimation method, impedance control is achieved and observed through changes in q and increased impedance control input τ_{imp}, whereas gravity compensation τ^p_{gc} only changes slightly as a result of shifting body posture. On the other hand, the direct sensor gravity compensation estimation τ^s_{gc}, calculated simultaneously for comparison purposes in Fig. 3(b), but not used in the impedance control, is equal to the summation of τ^p_{gc} and τ_{imp}. Thus demonstrating that the direct sensor method is unable to distinguish between gravitational forces and external forces, which makes it unsuitable as a gravity compensation estimation method for impedance control. This fact is confirmed in a separate simulation where the direct sensor method is used as the gravity compensation estimation method used in the impedance control, but the knee joints do not deviate from the set point when load is applied.

C. Experiments

To demonstrate the capabilities of the proposed gravity compensation method with impedance control on the actual robot, static posture experiments under different loading conditions are performed. The robot is placed standing with the hips and knees slightly bent and arms extended out with a bend at the elbows, as shown in Fig. 1. Varying loads are applied at the elbow joint by placing a combination of 1.2 and 2.5 kg weights inside a bag of negligible mass held up by a 1.3 kg bar placed across the arms. All joints are kept in place using high gain position control, whereas both hip joints are controlled using impedance control with desired stiffness $K_d = 100$ N/m and damping $D_d = 5$ Ns/m.

The robot is initially unloaded (NL). The first loading step L_0 places the 1.3 kg bar at the elbow joints. The load is then incremented according to the following steps: $L_1 = 2.5$ kg,

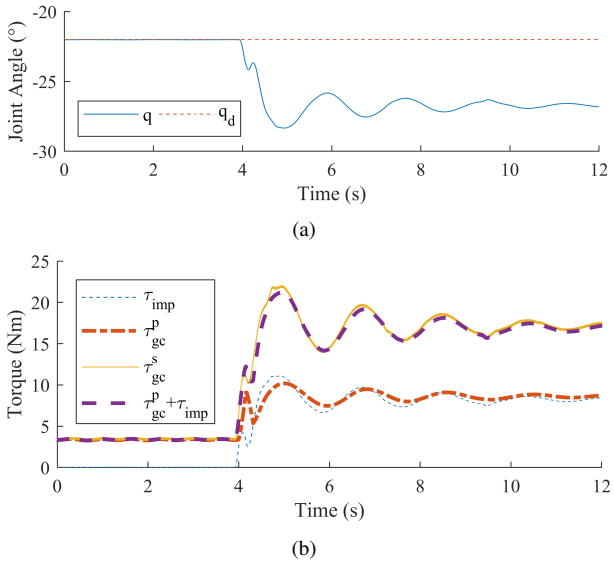

Fig. 3. Comparison of direct sensor and proportional method gravity compensation calculation for right knee joint: a) joint angle, and b) impedance control and gravity compensation torque values. Load applied at $t = 4$ s.

$L_2 = 5.0$ kg, $L_3 = 7.5$ kg, and finally $L_4 = 10.0$ kg. The entire load is then all removed from the robot in the final step. As seen in Fig. 4(a), the applied external force induces hip joint movement a result of impedance control. Increase in τ_{imp} correspond to changes in q. Large variances in τ_{gc} are also a result of the robot swaying and leaning during loading of the weights. Inconsistent changes in hip angles are a result of large amounts of joint friction, which can be observed in the difference in hip angles for both unloaded cases at $t = 0$ s and $t = 75$ s. Similar loading conditions in simulation lead to hip angle changes up to 6.5°, versus 2.5° on the actual robot. While the differences in angle between simulation and the actual robot is fairly large and attributed to joint friction, the results still demonstrate that impedance control is achieved using the proportional method.

Experiments are repeated using direct sensor method and regular high gain position control, and, as stated above, there are no significant changes in hip angle as the weights are loaded onto the robot. Furthermore, to confirm what was observed in simulation, variance is measured at different points and compared between the direct sensor method and proportional method. During stationary portions of the experiment, the proportional method achieved reductions in τ_{gc} signal variance ranging from 33% to 85% compared to the direct sensor method.

The use of model mass properties and relative F/T sensor values assumes that the limbs always bear the entire weight of the robot. Thus, problems arise while the robot is placed on the ground during initialization of experiments. Assistance from support scaffolding will cause the proportional method to generate incorrect τ^p_{gc} values that are too large for the actual load on the feet until the scaffolding no longer supports the robot. This issue is circumvented by creating an initialization phase that only uses 40% of the robot mass for

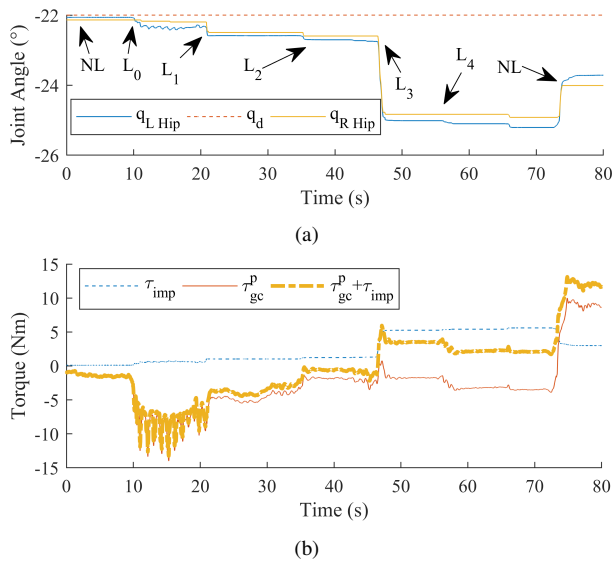

Fig. 4. Static posture experiments with HRP-4 robot under various loading conditions: a) joint position and b) right hip torque values. NL = 0 kg, $L_0 = 1.3$ kg, $L_1 = 2.5$ kg, $L_2 = 5.0$ kg, $L_3 = 7.5$ kg, $L_4 = 10.0$ kg

τ_{gc}^{p} calculations to allow the legs to collapse while lowering the robot until both feet contact the ground. The proportional method then slowly transitions to use 100% of the robot mass for τ_{gc}^{p} calculations.

IV. Conclusion

Gravity compensation estimation methods that directly use force and torque sensor values may not be reliable and are unsuitable for impedance control as they are unable to distinguish between gravitational and external forces. In this paper, a novel simple and straightforward method for gravity compensation estimation for multi-contact impedance control by combining model mass properties with relative F/T sensor data to estimate contact forces is proposed. The proposed method is able to implicitly distinguish between gravitational and external forces, and is also more robust to sensor errors such as noise, misalignment, and scaling. The application and improvements of the proportional method are verified using the humanoid robot HRP-4 both in simulation and real world experiments. Impedance control is demonstrated using static loading experiments, where hip joint angle changes are observed when an external load is applied to the robot. Simulation and experiments demonstrate the improved robustness of the proposed proportional method in calculating gravity compensation torque. As this work presents the precursor to implementing impedance controlled whole body motions, ongoing and future work includes determining the effect of model errors on the proposed method, comparisons to established contact force optimization methods, implementing full body impedance control, and extending the proportionality paradigm to bipedal robot balancing to improve robot stability during whole body motions.

Acknowledgment

This work was supported by Grant-in-Aid for Japan Society for the Promotion of Science (JSPS) Research Fellow PE17052. Special thanks to Shimpei Masuda and Kenya Mori for their help in performing experiments.

References

[1] L. J. Wood, A. Zaraki, M. L. Walters, O. Novanda, B. Robins, and K. Dautenhahn, "The iterative development of the humanoid robot kaspar: An assistive robot for children with autism," in *Social Robotics*. Springer International Publishing, 2017, pp. 53–63.

[2] A. Bolotnikova, K. Chappellet, A. Paolillo, A. Escande, G. Anbarjafari, A. Suarez-Roos, P. Rabate, and A. Kheddar, "A circuit-breaker use-case operated by a humanoid in aircraft manufacturing," in *2017 13th IEEE Conference on Automation Science and Engineering (CASE)*, Aug 2017, pp. 15–22.

[3] S. Nakaoka, A. Nakazawa, F. Kanehiro, K. Kaneko, M. Morisawa, H. Hirukawa, and K. Ikeuchi, "Learning from observation paradigm: Leg task models for enabling a biped humanoid robot to imitate human dances," *The International Journal of Robotics Research*, vol. 26, no. 8, pp. 829–844, 2007.

[4] T. Ito, K. Ayusawa, E. Yoshida, and H. Kobayashi, "Human motion reproduction by torque-based humanoid tracking control for active assistive device evaluation," in *2017 IEEE-RAS 17th International Conference on Humanoid Robotics (Humanoids)*, Nov 2017, pp. 503–508.

[5] K. Ayusawa and E. Yoshida, "Motion retargeting for humanoid robots based on simultaneous morphing parameter identification and motion optimization," *IEEE Trans. on Robotics*, vol. 33, no. 6, pp. 1343–1357, 2017.

[6] Y. Imamura, K. Ayusawa, E. Yoshida, and T. Tanaka, "Evaluation framework for passive assistive device based on humanoid experiments," *International Journal of Humanoid Robotics*, vol. 15, no. 03, 2018.

[7] A. Calanca, R. Muradore, and P. Fiorini, "A review of algorithms for compliant control of stiff and fixed-compliance robots," *IEEE/ASME Transactions on Mechatronics*, vol. 21, no. 2, pp. 613–624, April 2016.

[8] H.-O. Lim, S. A. Setiawan, and A. Takanishi, "Position-based impedance control of a biped humanoid robot," *Advanced Robotics*, vol. 18, no. 4, pp. 415–435, 2004.

[9] N. Hogan, "Impedance control: An approach to manipulation: Part iiimplementation," *Journal of dynamic systems, measurement, and control*, vol. 107, no. 1, pp. 8–16, 1985.

[10] K. Ayusawa, G. Venture, and Y. Nakamura, "Identifiability and identification of inertial parameters using the underactuated base-link dynamics for legged multibody systems," *The International Journal of Robotics Research*, vol. 33, no. 3, pp. 446–468, 2014.

[11] S. Ito, S. Nishio, Y. Fukumoto, K. Matsushita, and M. Sasaki, "Gravity compensation and feedback of ground reaction forces for biped balance control," *Applied bionics and biomechanics*, vol. 2017, 2017.

[12] S. H. Hyon, J. G. Hale, and G. Cheng, "Full-body compliant human-humanoid interaction: Balancing in the presence of unknown external forces," *IEEE Transactions on Robotics*, vol. 23, no. 5, pp. 884–898, Oct 2007.

[13] S. H. Lee and A. Goswami, "Ground reaction force control at each foot: A momentum-based humanoid balance controller for non-level and non-stationary ground," in *2010 IEEE/RSJ International Conference on Intelligent Robots and Systems*, Oct 2010, pp. 3157–3162.

[14] C. Ott, M. A. Roa, and G. Hirzinger, "Posture and balance control for biped robots based on contact force optimization," in *2011 11th IEEE-RAS International Conference on Humanoid Robots*, Oct 2011, pp. 26–33.

[15] A. Mifsud, M. Benallegue, and F. Lamiraux, "Estimation of contact forces and floating base kinematics of a humanoid robot using only inertial measurement units," in *2015 IEEE/RSJ International Conference on Intelligent Robots and Systems (IROS)*, Sept 2015, pp. 3374–3379.

[16] K. Kaneko, F. Kanehiro, M. Morisawa, K. Akachi, G. Miyamori, A. Hayashi, and N. Kanehira, "Humanoid robot HRP-4 - humanoid robotics platform with lightweight and slim body," in *2011 IEEE/RSJ International Conference on Intelligent Robots and Systems*, Sept 2011, pp. 4400–4407.